Astron. Astrophys. 362, 1072–1076 (2000)

ASTRONOMY AND ASTROPHYSICS

Mars: the role of water ice clouds on surface remote sensing

G. Bellucci

C.N.R., Istituto di Fisica dello Spazio Interplanetario, 00133 Rome, Italy (Giancarlo.Bellucci@ifsi.rm.cnr.it)

Received 17 March 2000 / Accepted 25 May 2000

Abstract. The possible effect of water ice clouds on spectroscopic measurements of the martian surface is evaluated. We have analysed imaging spectroscopic data of Mars in the 0.4–1.05 μm wavelength domain, obtained during the opposition in March 1997. The images show the classical albedo units in the red, while in the blue the surface contrast almost vanishes. Condensates on Hellas, north pole, Elysium and Acidalia, probably due to H_2O ice crystals, are visible in the blue images. Spectral analysis shows the presence of an effect, named "albedo reversal", occurring on Syrtis Major, Vastitas Borealis and Elysium. While this effect has been historically attributed to the spectral properties of the surface, from our study it appears that an atmosphere contribution could exist. We attribute the enhanced UV–VIS brightness to phase properties of airborne dust-H_2O ice particles.

Key words: techniques: spectroscopic – planets and satellites: individual: Mars

1. Introduction

Most of our knowledge about Mars geology and surface mineralogy has been gathered by spectroscopy. In the visible–near infrared, the reflected spectrum of classical bright and dark regions show a deep absorption in the $0.3 \div 0.6$ μm. Mars spectral behavior is dominated by Fe mineralogy; Fe^{3+} is present in the dust and soil and poorly crystalline or nanophase ferric–bearing materials dominate the visible to near–IR spectral properties of Mars (Morris et al. 1985). More amorphous materials such as palagonite, have also been suggested as the surface materials. Crystalline ferric oxides such as hematite in a crystalline form have also been discovered on the basis of ground–based spectroscopic observations and spacecraft remote sensing measurements (Bell et al. 1992, Christensen et al. 1998). The albedo of classical surface markings is not constant over time probably due to seasonal and interannual variations of contrast between dark and bright regions (Slipher 1962, Baum 1974, Capen 1976, Martin et al. 1992, Bell et al. 1999). These effects are in general due to global dust storms and seasonal winds, which transport light–colored dust from some areas to others (Christensen 1988). A specific phenomenon linked to spectral properties of the soils is the contrast reversal, that is one region brighter than an other in the red light, appears darker at shorter wavelengths (Barth et al.1972, Thomas & Veverka 1986). Observations of contrast reversal have been reported by many investigators by means of ground–based observations (McCord 1969, Adams & McCord 1969, McCord & Westphal 1971, Thomson 1973). Regions involved are Syrtis Major, Arabia, Sinus Meridiani, Sinus Sabeus, Pandorae Fretum and Mare Serpentis. The analysis of Viking Orbiter images has demonstrated that contrast reversal can be a surface phenomenon associated to specific eolian features as intra–crater deposits and wind streaks originating from deposits (Thomas & Veverka 1986). However the instances of albedo reversal reported by ground based observers can be influenced by the scattering properties of the atmosphere at different viewing conditions. In particular, we point out the possible effect of water ice clouds on spectral remote sensing of Mars. In this paper we present the result of observations made by means of imaging spectroscopy instrumentation during the 1997 opposition.

2. Observations and data reduction

We observed Mars using an imaging spectrometer in the $0.4 \div 1.05$ μm spectral range on the 1.5 m telescope at Sierra Nevada Observatory, Granada (Spain), from 19 March through 24 1997. The planet was at a geocentric distance Δ = 0.659 AU with an angular dimension of 14.2″. The telescope was configured at f/8, yielding a scale of 0.4 arcsec per pixel, equivalent to a footprint of 186 Km. However, during the period of our observations, seeing rarely reached the 1″, while most of the period seeing was 2″. The spectrometer used a CCD detector, 384x288 pixels of 23×23 μm dimensions and cooled by liquid nitrogen at -40° C. The instrument simultaneously acquire contiguous high–resolution spatial and spectral information, thus producing a so–called image cube. The images were obtained scanning the telescope across the planet and acquiring each CCD frame. The frames were then packed into a tridimentional data set (e.g. image cube) composed of 121 monochromatic (bandpass $\Delta\lambda$ = 50 Å) images. The summary of the observations is reported in Table 1. We report the results of analysis of only one image cube because it presents the best signal to noise ratio. It was acquired on March 20 at 0.20 UT. Dark and flat field frames were acquired and the cubes corrected following standard procedures. The raw data were corrected for various instrumental effects

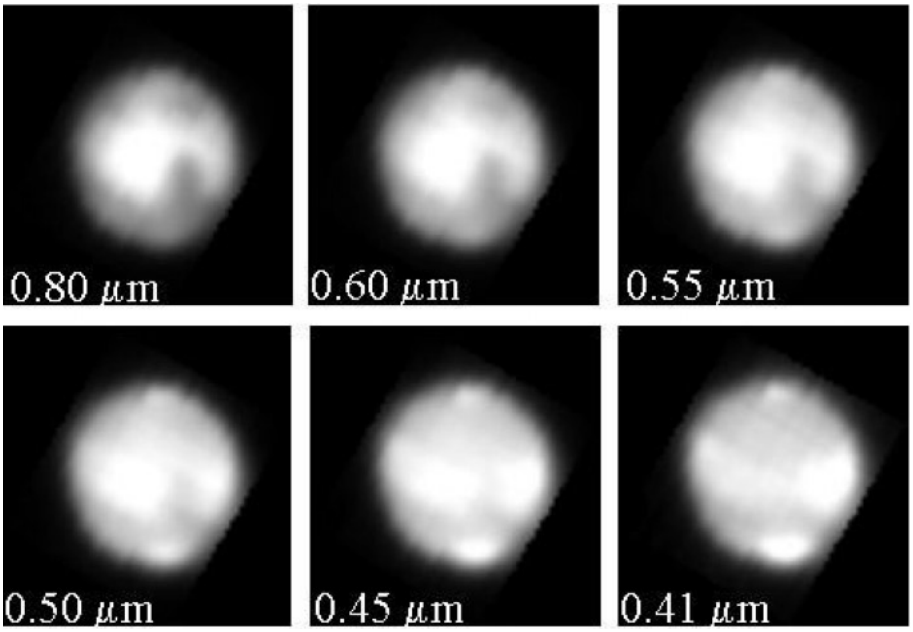

Fig. 1. Multispectral images of Mars acquired on March 20. The wavelength in micron is indicated.

following the procedures described in Bellucci et al. (1998). In order to correct the spectra for instrumental response and telluric absorption features, relative reflectance spectra were created by ratioing the raw spectra to the Mare Serenitatis II (MS2 18°40'N, 21°25'E) area on the Moon, which was observed at same Mars air mass and time. A residual telluric feature due to O_2 is however still present in the reduced spectra (see Fig. 2 below). Absolute reflectance spectra were then produced by using the following relation:

$$R = \frac{I_{\rm Mars}}{I_{\rm MS2}} \times S_{\rm MS2} \times C \quad (1)$$

where $I_{\rm Mars}$, $I_{\rm MS2}$ are the Mars and MS2 raw spectra, respectively, $S_{\rm MS2}$ is the reflectivity of MS2 (McCord et al. 1972) and C a scaling factor. C was chosen to scale the average spectrum of Arabia to 0.4 at 1.040 μm (Bell et al., 1999).

In Fig. 1 a reduced data set is shown in the form of six monochromatic images.

The corresponding wavelength (in micron) of each image is also shown. It was summer in the northern hemisphere of Mars at time of our observations (L_s = 92) and Syrtis Major, Hellas cloud and north pole were visible.

3. Results

With reference to Fig. 1, the classical bright and dark regions are well visible in the red images (λ = 0.8 μm), while the contrast almost vanish in the bluest. Condensates are visible on Hellas and North pole; limb clouds and equatorial haze are also visible. The lowering contrast of the Martian features at short wavelengths is due to the spectral characteristics of the iron oxides which dominate the Martian surface. As the wavelength becomes shorter and shorter, Syrtis Major tends to disappear while northern hemisphere becomes darker than the equatorial region and comparable in brightness to the south dark units. Any spatial detail in the northern hemisphere is completely lost, as can be seen by comparing the 0.41 μm image with the 0.8 μm, where a dark unit on Vastitas Borealis is visible. In summary, even a coarse examination of the data set in the form of multispectral images, shows the occurrence of contrast reversal in diverse regions of Mars. Let now focus our attention on the spectra. We have plotted in Fig. 2a spectra of the main albedo units of Mars visible in the red images. Each spectrum is an average of a 2×2 box centered on the area of interest; bright, intermediate and dark units have been sampled. Mean latitude, longitude, incidence and emission angles are shown in Table 2.

The spectra of low to intermediate albedo regions show a negative slope throughout the visible near infrared. In the 0.4–0.6 μm range, we clearly see the occurrence of crossover of the reflectance curves for some areas. In order to better identify the spectra at short wavelengths, another plot is shown in Fig. 2b, where spectra relative to Arabia are shown. For example, the spectrum of Elysium (brown) crosses the Arabia (yellow) at 0.519 μm, while the Elysium (dark green) crosses the Arabia (yellow) at 0.455 μm. The Utopia spectrum crosses the Syrtis Major (green) at 0.544 μm. Sinus Meridiani crosses Syrtis Major (green) at 0.519 μm and Acidalia-Vastitas at 0.485 μm. The two Elysium spectra cross themselves at 0.614 μm. Syrtis Major (green) crosses Arabia (yellow) at 0.425 μm. Other interesting findings are: 1) the coincidence of Sinus Meridiani and Syrtis Major (red) spectra in the 0.6–1 μm range while they diverge shortward of 0.598 μm; 2) the overlap of Hellas cloud-Syrtis Major (green) in the 0.6–1 μm range while they diverge shortward of 0.628 μm.

4. Interpretation

The findings presented above could be interpreted in terms of both surface and atmospheric features. Lack of contrast at short wavelengths has been attributed to the spectral properties

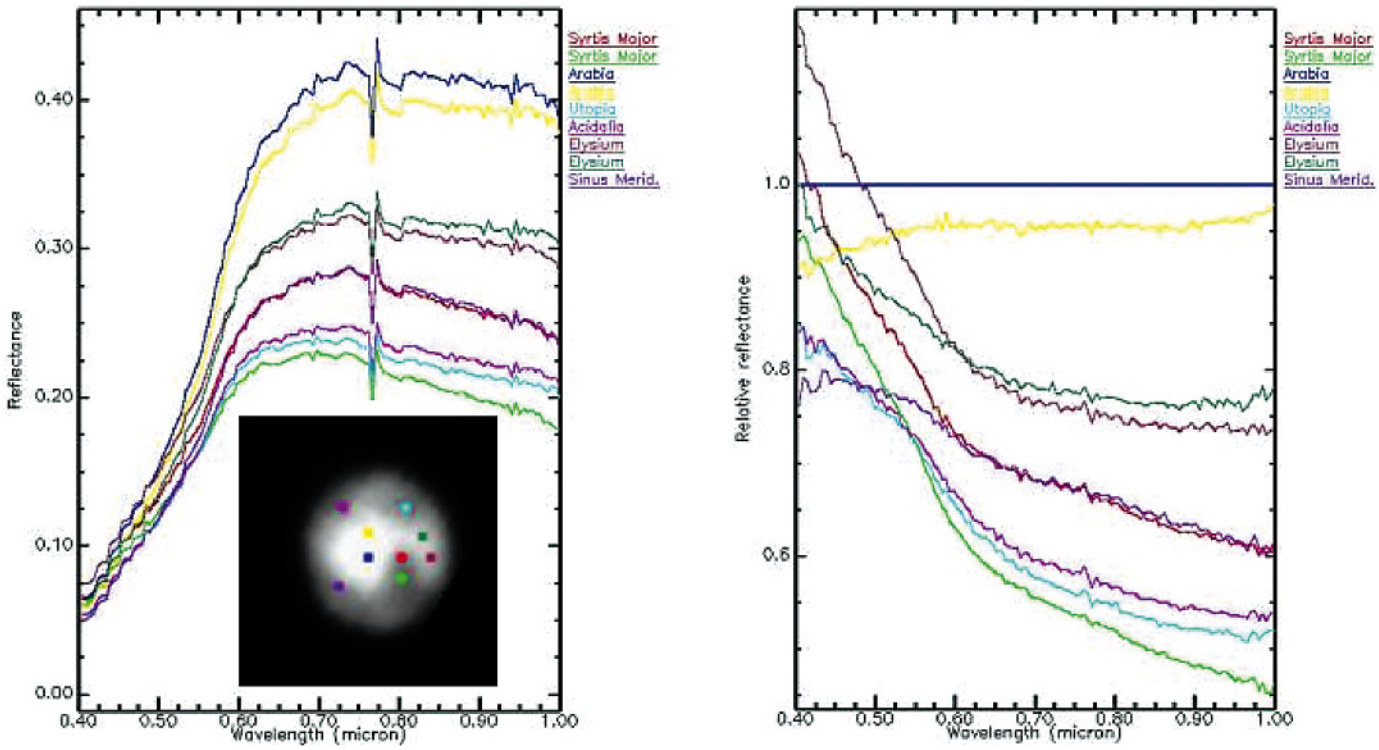

Fig. 2. Left panel shows the spectra of bright, intermediate and dark regions on Mars. Right panel: enlargement of the 0.4–0.6 μm region to show the occurrence of reflectance crossover. The spectra are represented as relative to the Arabia spectrum

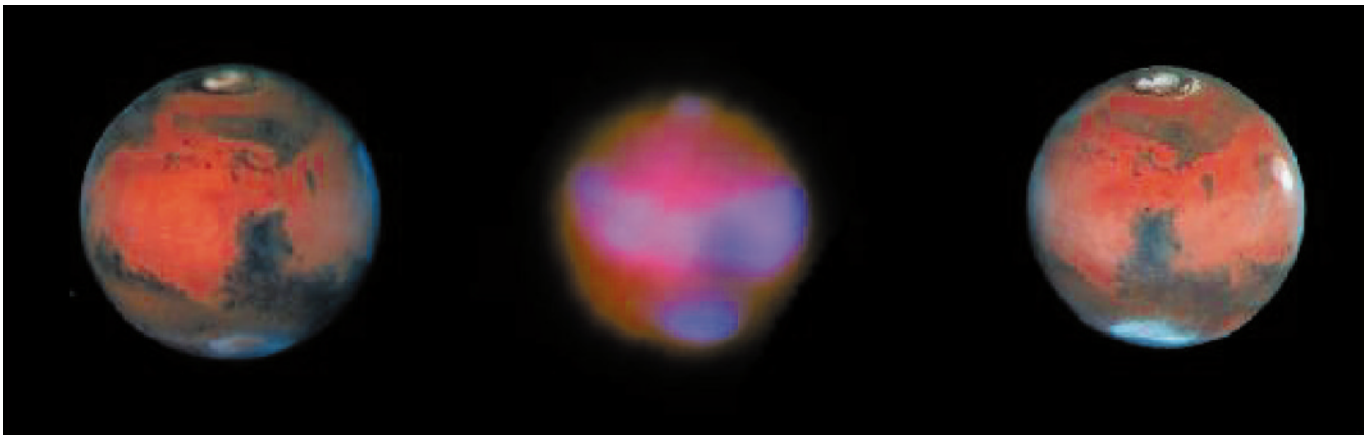

Fig. 3. Red, Green, Blue composite images of Mars during March 1997 (see text). They show limb clouds and an equatorial haze of H_2O ice. The left and the right images were taken by HST on 10 and 30 March, respectively. The image in the center was taken on 20 March by the author and it is discussed in the text.

of iron oxides (Huguenin et al. 1977). This can explain the lowering of contrast of Martian features observed in the northern hemisphere (Vastitas and Acidalia). Viking images have shown the occurrence of albedo reversal at regional scales ($<$ 300 Km) and it has been attributed to eolian deposits (Thomas & Veverka 1986). The classical contrast reversal phenomenon occurs among the Sinus Meridiani and Vastitas-Acidalia, with crossover appearing at 0.485 μm and Syrtis Major with Arabia, with crossover at 0.425 μm. The amount of reflectance increase at short wavelengths and position of crossover suggest that we are looking to some clouds or haze. Mars was observed during this opposition by the HST Wide field planetary camera. In Fig. 3, two color composite WFPC2 images taken on 10 and 30 March are shown. They are composed of individual red (673 nm), green (502 nm) and blue (410 nm) exposures. In the figure, a color composite at the same wavelengths obtained from our data is also shown. It has been stretched in order to have approximately the same color tint. It must be noted that the bandpass of the red and green WFPC2 camera filters are 5 and 3 nm, approximately the same of our spectrometer channels (5 nm). The blue filter has $\Delta\lambda$ = 14 nm; for this reason we have taken an average of the 405, 410, 415 channels to generate the

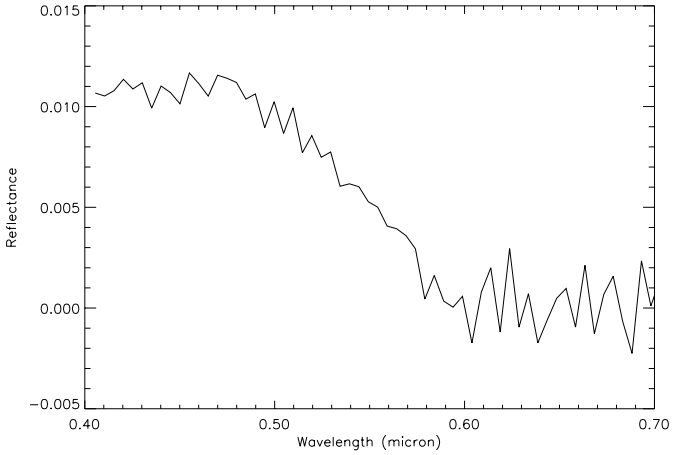

Fig. 4. Spectral dependence of brightening observed on Elysium. It has been obtained by subtracting a surface term to the cloud spectrum.

Table 1.

Date and Time	03/20/97 00.20 UT
Magnitude	-1.3
Sub-Earth point	314.2° lon 23° lat
Distance	0.659 AU
Phase	3.1°
Airmass	1.4
Ls	92

Table 2.

	Lat	Lon	i	e
Syrtis Major	10°-20°	290°	16°	19°
Utopia	50°	270°	36°	39°
Elysium	20°-35°	250°-260°	46°-56°	49°-59°
Arabia	20°-35°	320°	8°	11°
Sinus Meridiani	10°	350°	38°	41°
Acidalia	45°	10°	58°	61°

blue component in the Fig. 3 picture. On the WFPC2 images, a diffuse water ice haze is visible on the equatorial region. On the 30 March image it is more visible, probably due to a slightly different color stretch. Our image, taken on 20 March, shows a more prominent haze layer, which covers almost completely the Syrtis Major and Elysium regions while it is more diffused on Arabia. We have considered the limb cloud located approximately on Elysium as representative of the clouds and hazes visible on the blue images. The spectrum is an average of 4×4 pixels. In order to obtain the surface term, we sampled a spectrum at the same longitude of Elysium but just out of the cloud. We can assume that the surface close to the haze covered terrains has the same spectral response of the haze-underlying soils. The rationale of this approximation is due to the spectral homogeneity of bright regions, at least at the spatial scales involved in ground based observations. Fig. 4 shows the spectral dependence of brightening obtained by subtracting the surface spectrum to the cloud spectrum.

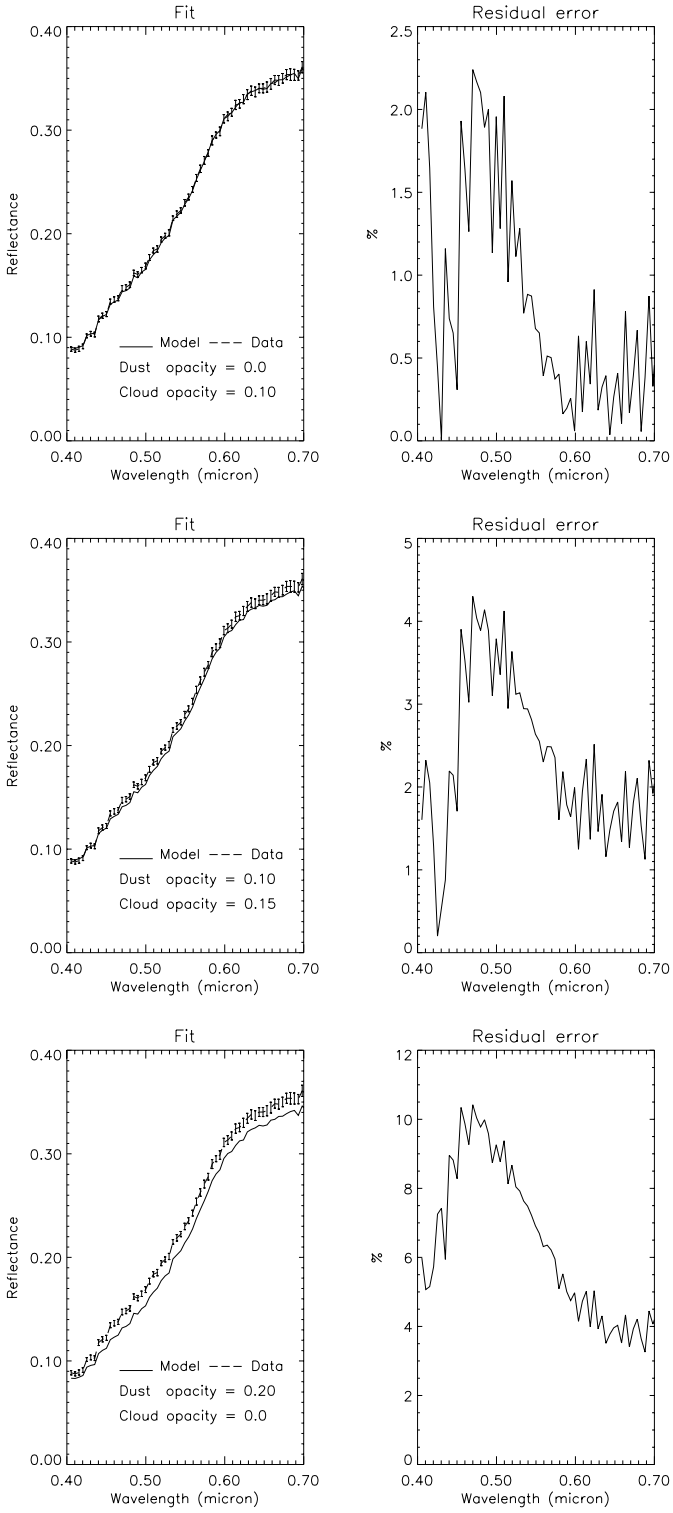

Fig. 5. Results of radiative transfer modeling of Elysium cloud. They have been obtained by using different dust and cloud opacities. See the text for details

The spectral brightening shown in Fig. 4 tends to be flat below 0.5 μm, with perhaps a small peak at 0.45 μm. We have modeled the observed spectral behavior in the 0.4–0.7 μm domain by using a discrete ordinates radiative transfer code

(Disort, Stamnes et al. 1988). The martian atmosphere has been subdivided in two layers (0–10 Km, 10–20 Km) which take into account the vertical distributions of dust, water clouds and CO_2 Rayleigh scattering, by taking a surface pressure of 7 mbar. Following Clancy et al. 1996a, we assume 60% of the cloud opacity occurs in 0–10 Km layer and the remaining 40% in the 10 -20 Km layer. The condensation level of Mars water vapor is specified by the aphelion atmospheric temperature profile (Clancy et al. 1996b). The ozone absorption occurring above 20 Km altitude has been negletted because it affects only wavelengths shorter than 0.3 μm. Cloud and dust single scattering phase functions are taken from results of Clancy & Lee 1991. The dust single scattering albedo is adopted from Wolf et al. 1999, while for the clouds it is fixed to 1. The cloud and dust opacities are treated as wavelenght independent parameters and varied to achieve a consistent macth to the observed spectra. From previous studies this appear to be a reasonable approximation (Clancy et al. 1995; Smith et al. 1997; Wolff et al. 1999). Fig. 5 shows the results. The best fit to the data points has been obtained with a cloud opacity τ_c = 0.10 and dust opacity τ_d = 0. The residual is below 3% in the all wavelength range. Anyway, a model compatible with the data error bar is also obtained, by taking τ_c = 0.10 and τ_d = 0.15, through with a poorer fit. As shown in Fig. 5b, the residual is now larger, specially in the $0.5 < \lambda < 0.7$ μm domain. The case of a "pure" dusty atmosphere is shown in Fig. 5c. The figure shows how it is necessary to include some ice opacity to decrease the overall error fit. In summary, even though modelling pushes toward a dust free atmosphere, an higher dust opacity is not excluded. Wolff et al. 1999 report a diffuse dust opacity value τ_d = 0.3, measured at the end of March. Recently, the role of water ice clouds on martian climate has been revaluated. Clancy et al. 1996b showed the occurrence of low altitude (10 km) water vapor saturation around several Mars aphelions. During these periods the Mars atmosphere was 15–20 K colder than observed during the Viking mission. At these temperatures, water ice clouds form at low altitude, covering the 10°S - 30°N latitude region (James et al. 1994, Clancy et al. 1996b, Wolff et al. 1997). Temperatures 40 K lower than Viking mission were also reported by Pathfinder (Magalhães et al. 1999). An inversion at about 10 Km has been also observed which can lead to the formation of low-altitude clouds (Colaprete et al. 1999). In the 1997 opposition Mars was close to the aphelion and the same scenario probably occurred. We then suggest that the albedo reversal observed in our spectra and relative to several region of Mars, mainly located in the equatorial belt, is due to the scattering properties of low altitude water ice clouds. If the clouds condense around dust as nucleation centers, fine dust particles can be transported from one region to another, contributing to albedo variation of surface markings. Instances of albedo reversal reported by ground-based observers in the past could also be explained by the presence of low altitude water ice clouds (McCord 1969). On the other hand, occurrence of this phenomenon was reported also when Mars was much closer to the Sun (Thompson 1973). In this case, water ice clouds forming at higher altitudes could be invoked to explain the observations. Generally, the albedo features involved are located at equatorial–tropical latitudes. There is no clear evidence of a seasonal dependence of the reversal, mainly due to the sparse observations (Martin et al. 1992).

Acknowledgements. I thank Dr. J. L.Moreno and Dr. J. Rodrigueez of Institute of Astrophysics of Andalucia for their assistance. The author wishes to thank Dr. M. Wolff for his detailed review that resulted in a substantial improvement respect to the earlier version of manuscript. The help of Mrs. S. Zampieri in the manuscript preparation is also acknowledged. Funding were provided by ASI and CSIC grants.

References

Adams J. B., McCord T. B., 1969, J. Geophys. Res. 74, 4851
Baum W. A., 1974, Icarus 22, 263
Barth C. A., Hord C.W., Stewart A.I., Lane A.L., 1972, Data Report 4, LASP, Univ. of Colorado
Bellucci G., 1998, Planet. Space. Sci. 46,377
Bell J. F., 1992, Icarus 100, 575
Bell J. F., Wolff M.J., Daley T.C., et al., 1999, Icarus 138, 25
Capen C. F., 1976, Icarus 28, 213
Clancy R. T., Lee S. W., 1991, Icarus 93, 135
Clancy R. T., Lee S. W., Gladstone G. R., McMillan W.W., Rousch T., 1995, J. Geophys. Res., 100, 5251
Clancy R. T., Wolff M.J., James P.B., et al., 1996a, J. Geophys. Res., 101, 12777
Clancy R. T., Grossman A.W., Wolff M.J., et al., 1996b, Icarus 122, 36
Colaprete A., Toon O.B., Magalhães J. A., et al., 1999, J. Geophys. Res., 104, 9043
Christensen P. R., 1988, J. Geophys. Res., 93, 7611
Christensen P. R., Anderson D.L., Chase S.C., et al., 1998, Science 279, 1692
Huguenin R. L., Adams J.B., McCord T.B., 1977, Lunar Sci., VII, 478
James P. B., Clancy R.T., Lee S.W., et al., 1994, Icarus 109, 79
Magalhães J. A., Schofield J.T., Seiff A., et al., 1999, J. Geophys. Res., 104, 8943
Martin L. J., James P.B., Dollfus A., Iwasaki K., Beish J.D., 1992, Mars (Univ. of Arizona press Tucson), 34
McCord T. B., 1969, ApJ, 156, 79
McCord T. B., Westphal J. A., 1971, ApJ, 168, 141
McCord T. B., Charette M.P., Johnson T.V., et al., 1972, J. Geophys. Res., 77, 1349
Morris R. V., Lauer H.V.Jr., Lawson C.A., et al., 1985, J. Geophys Res. 90, 3126
Slipher E. C., 1962, The Photographic story of Mars (eds. Flagstaff: Northland Press.)
Smith P. H., Bell J.F.III, Bridges N.T., et al., 1997, Science 278, 1758
Stamnes K., Tsay S.-C., Jayaweera K., Wiscombe W., 1988, Appl. Opt. 27, 2502
Thomas P., Veverka, J., 1986, Icarus 66, 39
Thompson D. T., 1973, Icarus 20, 42
Wolff M. J., Lee S.W., Clancy R.T., et al., 1997, J. Geophys Res. 102, 1679
Wolff M. J., Bell III J.F., James P.B., Clancy R.T., Lee S.W., 1999, J. Geophys Res. 104, 9027